Correlated Perovskites as a New Platform for Super-Broadband-Tunable Photonics

Zhaoyi Li, You Zhou, Hao Qi, Qiwei Pan, Zhen Zhang, Norman Nan Shi, Ming Lu, Aaron Stein, Christopher Y. Li, Shriram Ramanathan, and Nanfang Yu**

Strongly correlated perovskites possess widely tunable electronic structure that can host a variety of phases. Nickelates, in particular, undergo electric-field-tunable phase transitions with dramatic changes in the optical properties. We experimentally demonstrate strong optical modulation utilizing the large and non-volatile optical refractive index change associated with electron-doping induced phase change of a prototypical perovskite, $SmNiO_3$. Large electrical modulation of light over a broad wavelength range, from the visible to the mid-infrared, λ = 400 nm to 17 μm, is demonstrated using thin-film $SmNiO_3$. By integrating $SmNiO_3$ into plasmonic metasurface structures, modulation of a narrow band of light that resonantly interacts with the metasurfaces is realized. Furthermore, we demonstrate solid-state electro-optic modulators by integrating $SmNiO_3$ and solid polymer electrolytes. Correlated perovskites with tunable and non-volatile electronic phases create a new platform for active photonic devices, such as electro-optic modulators, electrically programmable optical memories, smart windows for controlling sunlight, and variable emissivity coatings for infrared camouflage and thermoregulation.

There has been persistent exploration of new tunable materials and novel device architectures to dynamically control light with larger modulation depth and increased spectral range, at faster speed, and using less power. Optical modulators prevailing in today's consumer-based optical products are typically based on weak nonlinear electro-optic phenomena, such as Pockels effect, optical Kerr effect, and plasma-dispersion effect.[1,2] These devices require either high operation voltages or large device footprints to achieve large modulation depth, and are therefore unsuitable for the increasingly demanding requirements of device miniaturization and large-scale integration in modern photonic systems. A small electro-optic effect can be amplified to realize large optical modulation in a narrow spectral range by using high-quality-factor optical resonators. For example, fast telecomm electro-optic modulators have been demonstrated based on free carrier injection in silicon microresonators.[3,4]

Large changes in complex refractive indices can be induced in thin-film materials such as indium tin oxide and graphene using field effect.[5–9] However, a significant refractive index change can only occur over small volumes, and nanophotonic structures have to be used to enhance light–material interaction. Electrochromic materials, such as transition metal oxides and conjugated conducting polymers, show large and reversible changes of color during electrochemical redox reactions.[10,11] However, the change of optical refractive indices is diminishingly small as the wavelength increases. For example, perhaps the most widely studied electrochromic material WO_3 can provide large modulation of light in the visible and near-infrared but the modulation depth in the long-wavelength mid-infrared, λ = 8–20 μm, is very limited.[12] Similarly, organic electrochromic materials provide limited optical modulation in the mid-infrared due to various molecular vibrational transitions in the organic molecules.[13,14]

Phase-change materials such as chalcogenide alloys that have been used in rewritable CDs, DVDs, and Blu-ray discs, can be switched between the amorphous and crystalline states by laser or electrical current pulses with controlled duration and intensity.[15,16] This material system has recently been used to demonstrate all-optical, multi-level, and non-volatile memory in telecomm integrated photonic circuits,[17] high-resolution solid-state displays,[18] and optically reconfigurable planar optical components.[19] However, chalcogenide alloys have large absorption coefficients in the visible and are therefore not suitable for modulating visible light.

In the materials systems described above, optical-refractive-index changes either have limited magnitude, or significant refractive index changes can only occur within limited wavelength range or over limited spatial volume (see Figure S7 and S8, Supporting Information, for a comparison of different tunable optical materials). In this paper, we report experimental results demonstrating that $SmNiO_3$, a prototypical phase-change perovskite nickelate, exhibits large and reversible refractive index changes over an ultrabroad spectral range, from the

Z. Li, N. N. Shi, Prof. N. Yu
Department of Applied Physics and Applied Mathematics
Columbia University
New York, NY 10027, USA
E-mail: ny2214@columbia.edu
Dr. Y. Zhou
Department of Chemistry and Chemical Biology
Harvard University
Cambridge, MA 02138, USA
H. Qi, Dr. Q. Pan, Prof. C. Y. Li
Department of Materials Science and Engineering
Drexel University
Philadelphia, PA 19104, USA
Dr. Z. Zhang, Prof. S. Ramanathan
School of Materials Engineering
Purdue University
West Lafayette, IN 47907, USA
E-mail: shriram@purdue.edu
Dr. M. Lu, Dr. A. Stein
Center for Functional Nanomaterials
Brookhaven National Laboratory
Upton, NY 11973, USA

DOI: 10.1002/adma.201601204

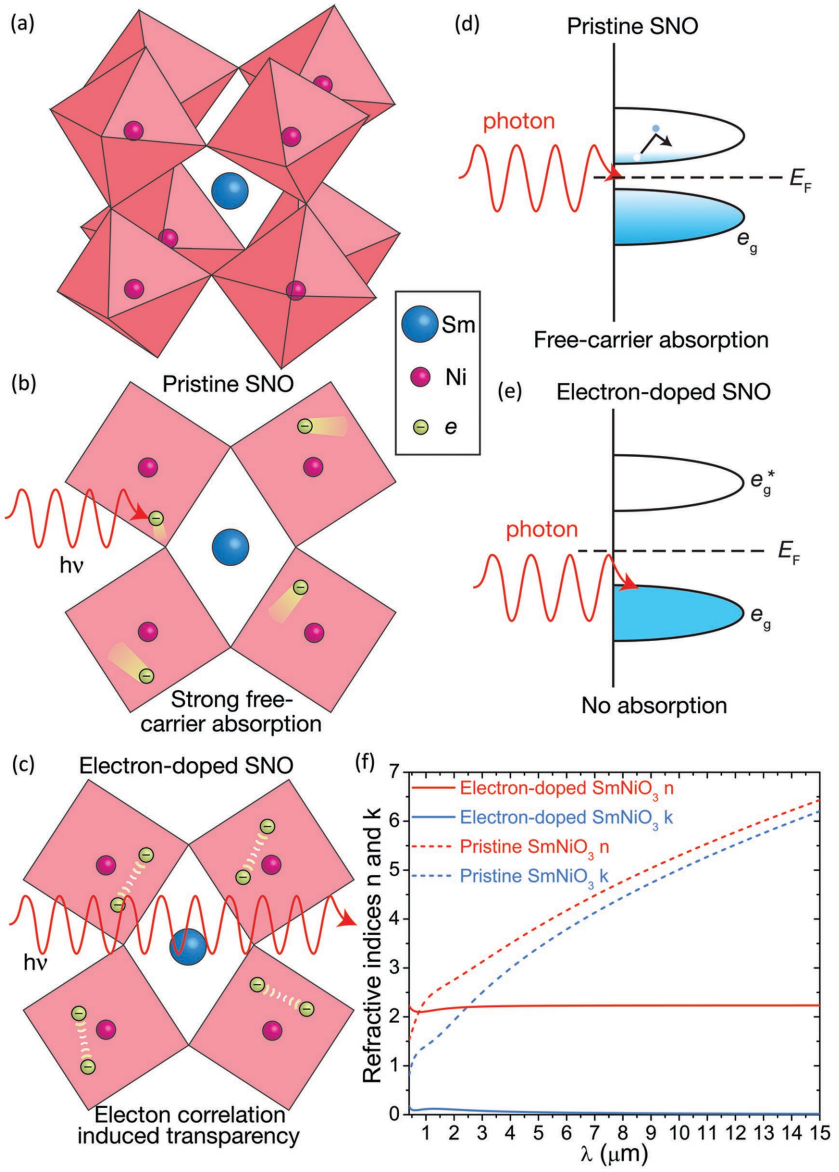

Figure 1. Electron-doping-induced phase transition of $SmNiO_3$. a) Perovskite structure of $SmNiO_3$. Each vertex of the octahedra represents one oxygen atom. b) In pristine $SmNiO_3$, electrons are itinerant because of the single occupancy of the Ni e_g orbital, and cause strong free-carrier absorption. c) When each NiO_6 octahedra is doped with one more electron, strong Coulomb repulsion leads to electron localization and the interaction between electrons and photons is suppressed. d) The conduction band of pristine $SmNiO_3$ is populated with free electrons, which lead to strong free-carrier absorption. e) Strong electron correlation in doped $SmNiO_3$ opens up a wide bandgap and eliminates the free electrons. In (d) and (e), the horizontal axis represents the density of states and the vertical axis represents energy; e_g* in (e) means the antibonding state of the e_g orbital (i.e., the upper Hubbard band). f) Complex refractive indices (n and k) extracted from experiments. Pristine $SmNiO_3$ has high electrical conductivity and is optically opaque. Electron-doped $SmNiO_3$ is electrically insulating and optically transparent. The electron doping process (doping concentration of the order of 0.1–1 carriers per unit cell, or ≈10^{21}–10^{22} cm^{-3}) can be induced via several approaches including gas phase, liquid phase, and solid-state dopant injection. Photonic devices based on all of these approaches are presented in this study for the sake of completeness.

visible to the long-wavelength mid-infrared (λ = 400 nm to 17 μm). The super broadband performance is due to strong electron correlation effects that allow extraordinarily large band gap tuning of the order of 3 eV, and this new mechanism can be exploited to create a variety of active photonic devices.

The electronic phase diagram of correlated perovskite nickelates is very sensitive to orbital occupancy of electrons (**Figure 1**). In particular, $SmNiO_3$ exhibits reversible modulation of electrical resistivity greater than eight orders of magnitude and an order of magnitude change in optical band gap at room temperature during an electron-doping-induced phase transition.[20] In pristine $SmNiO_3$, Ni^{3+} has an electron configuration of $t_{2g}^6e_g^1$ and the single e_g electron causes strong optical losses through free carrier absorption (Figure 1b), which is characterized by a large imaginary part, k, of the complex refractive index (Figure 1f). By acquiring an extra electron, the fourfold degenerate (including spin) e_g manifold is occupied by two electrons. The strong intra-orbital Coulomb repulsion between e_g electrons opens a band gap as large as 3 eV and almost completely suppresses the free carrier absorption (Figure 1c). Thus, $SmNiO_3$ is transformed into an optically transparent dielectric with $n \approx 2.2$ and k close to zero throughout the visible, near-infrared, and mid-infrared (Figure 1f). The drastic change in the optical properties upon electron-doping can also be understood on the basis of the change in the density of states near the Fermi level (Figure 1d,e). The switching between the two states can occur at room temperature in a nonvolatile fashion and the two states have no obvious differences in their crystalline symmetry (within the detection limits of X-ray and electron diffraction) (Figure 1a and Section S1, Supporting Information).[20–22] These desirable properties open up the opportunity to realize electrically tunable, nonvolatile, planar photonic devices at any wavelength from the visible to the mid-infrared. Note that $SmNiO_3$ is different from electrochromic materials in terms of the mechanism of color change. The phase transition of $SmNiO_3$ is a result of strong electron correlation, which is a collective quantum effect, while conventional electrochromic materials are based on redox reactions. The major consequence is that electron doping makes many electrochromic materials more conductive, whereas $SmNiO_3$ becomes insulating with electron doping due to charge carrier localization.

We realized tunable photonic devices based on several different architectures and utilizing a range of techniques to induce the doping-driven phase transition of $SmNiO_3$ (summarized in Figure S1, Supporting Information). In brief,

Adv. Mater. **2016**,
DOI: 10.1002/adma.201601204

experimentally demonstrated devices include: i) devices based on thin-film $SmNiO_3$ providing large and broadband tuning of optical transmissivity, reflectivity, and emissivity, where the phase transition of $SmNiO_3$ is induced by lithium intercalation and de-intercalation, or hydrogenation and de-hydrogenation; these devices have potential applications in smart windows and variable emissivity coatings; ii) devices based on plasmonic metasurfaces patterned on thin-film $SmNiO_3$ providing large tuning of reflectivity over a narrow band of wavelengths, where the phase transition is realized by ionic liquid gating, or hydrogenation and de-hydrogenation; these devices have potential applications in optical modulators and optical memories; iii) solid-state devices based on thin-film $SmNiO_3$ and a solid polymer electrolyte providing broadband modulation of reflectivity and represent a new platform for active solid-state photonic devices.

In the first set of experiments, we demonstrated large tuning of visible and near-infrared transmissivity using 80 nm $SmNiO_3$ thin films epitaxially grown on $LaAlO_3$ substrates (**Figure 2**a,b). The phase transition of $SmNiO_3$ was realized by lithium intercalation and de-intercalation (Section S2.1, Supporting Information). An electrolyte containing lithium ions was added on the surface of $SmNiO_3$ and a voltage was applied between $SmNiO_3$ and a lithium electrode to drive ion transport. The lithium ions adsorbed on the surface and doped in $SmNiO_3$ facilitate the incorporation of electrons into $SmNiO_3$, which triggers the phase transition of $SmNiO_3$. A voltage with reverse polarity pulls lithium ions back to the electrolyte and the $SmNiO_3$ film is thereby converted back to the pristine state.

The measured transmission spectra (Figure 2b) show that the averaged transmissivity of the device with intrinsic $SmNiO_3$ over the wavelength range of 400–1000 nm is ≈0.04. When $SmNiO_3$ is in the electron-doped state (i.e., complete lithium intercalation), however, the averaged transmissivity increases drastically to ≈0.39, where optical losses are mostly caused by the $LaAlO_3$ substrate (i.e., $LaAlO_3$ contributes to ≈73% of absorption). The tuning of transmissivity averaged in the visible (λ = 400–700 nm) is ≈0.35. The large tuning of visible light transmission is further illustrated in Figure 2a, which is an optical image of the device put on top of a Columbia Engineering School logo to show different degrees of transparency corresponding to $SmNiO_3$ at its intrinsic state and at different stages of electron doping (additional optical images are provided in Section S3, Supporting Information).

In the second set of experiments, we demonstrated large and reversible changes to the near-infrared and mid-infrared spectra using thin-film $SmNiO_3$ (Figure 2c–h). We took transmission and reflection spectra of a 200 nm $SmNiO_3$ film deposited on a 1 μm suspended Si_3N_4 membrane after removing the electrolyte containing lithium ions at the end of each electrochemical reaction. Measured transmission spectra show large and reversible tuning of transmissivity over a broad spectral range (Figure 2d,g). The transmissivity of pristine $SmNiO_3$ is below 0.05 in the near-infrared (wavenumber ν, from 4000 to 10 000 cm^{-1}, or wavelength λ, from 1 to 2.5 μm) and below 0.17 in the mid-infrared (ν = 600–4000 cm^{-1}, or λ = 2.5–16.7 μm) (Figure 2d). Electron-doped $SmNiO_3$, however, becomes optically transparent with transmissivity around 0.7, except for a pronounced dip around ν = 1000 cm^{-1} or λ = 10 μm (Figure 2d), which is due to optical absorption as a result of the phonon resonance in Si_3N_4. By switching $SmNiO_3$ between its opaque and transparent state, we were able to tune optical transmissivity by a factor as large as ≈270 at ν = 9000 cm^{-1} or λ = 1.1 μm and by a factor larger than 10 at ν > 2000 cm^{-1} or λ < 5 μm.

When $SmNiO_3$ is in the transparent state, both the transmission and reflection spectra are superimposed with Fabry–Pérot fringes (Figure 2d,e), indicative of thin-film interference. We were able to reach anti-reflective conditions (reflectivity < 0.01) at six different wavelengths (Figure 2e) and tuning of optical reflectivity at these wavelengths reaches maxima (Figure 2h). We were also able to significantly tune optical absorptivity, defined as (1 − reflectivity − transmissivity), for wavelengths smaller than 8 μm (Figure 2f). This implies that the device is capable of providing tunable thermal emission at λ < 8 μm as Kirchhoff's law of thermal radiation states that wavelength-specific emissivity equals to absorptivity.[23]

Experimental results very similar to those shown in Figure 2 were also obtained in $SmNiO_3$ thin films, where the phase transition was induced by hydrogenation/de-hydrogenation (or proton intercalation/de-intercalation). The device consists of a Pt grating patterned on a $SmNiO_3$ film, which was deposited on a suspended Si_3N_4 membrane (**Figure 3**a,b). The Pt grating serves as the catalyst for the hydrogenation process, in which H_2 molecules dissociate to atomic hydrogen, and further split into protons and electrons that are incorporated into the $SmNiO_3$ film. The device was annealed in O_3 to reverse the phase transition. Measured transmissivity is below 0.1 over the entire infrared spectrum when $SmNiO_3$ is in its pristine or de-hydrogenated state, and can be up to 0.85 for hydrogenated $SmNiO_3$ (Figure 3c). The optical transmissivity can be tuned by a factor larger than 20 for λ < 5 μm (Figure 3d). Large tuning of optical reflection occurs at several wavelengths corresponding to Fabry–Pérot resonances (Figure 3e,f).

As the speed of bulk phase transition is inversely proportional to the total volume of $SmNiO_3$ being switched (since the electron doping process is diffusional in nature beyond the screening length), one has to use ultrathin $SmNiO_3$ films in order to achieve, for example, high-speed optical modulation and high-speed programming of optical memory. However, as the amount of phase-change material is reduced, the magnitude by which light can be modulated decreases. The challenge is therefore maximizing modulation strength while simultaneously minimizing the amount of phase-change materials used. The challenge can be solved by integrating $SmNiO_3$ into metasurface structures, which consist of 2D arrays of densely packed optical antennas with subwavelength dimensions,[24–26] and are able to mediate strong light–material interactions on a 2D plane.

We successfully fabricated metasurface structures on $SmNiO_3$ films and demonstrated tuning of reflected light in a narrow band of mid-infrared spectrum (**Figure 4**). The metasurface modulator is based on a 2D array of cross-shaped platinum (Pt) aperture antennas (i.e., cross-shaped voids cut in Pt thin films) (Figure 4c) patterned on a substrate consisting of, from top to bottom, thin films of $SmNiO_3$, SiO_2, and Pt (Figure 4a). We used two methods to induce phase change of $SmNiO_3$: hydrogenation/de-hydrogenation (Section S2.2, Supporting Information) and ionic liquid gating (Section S2.3, Supporting

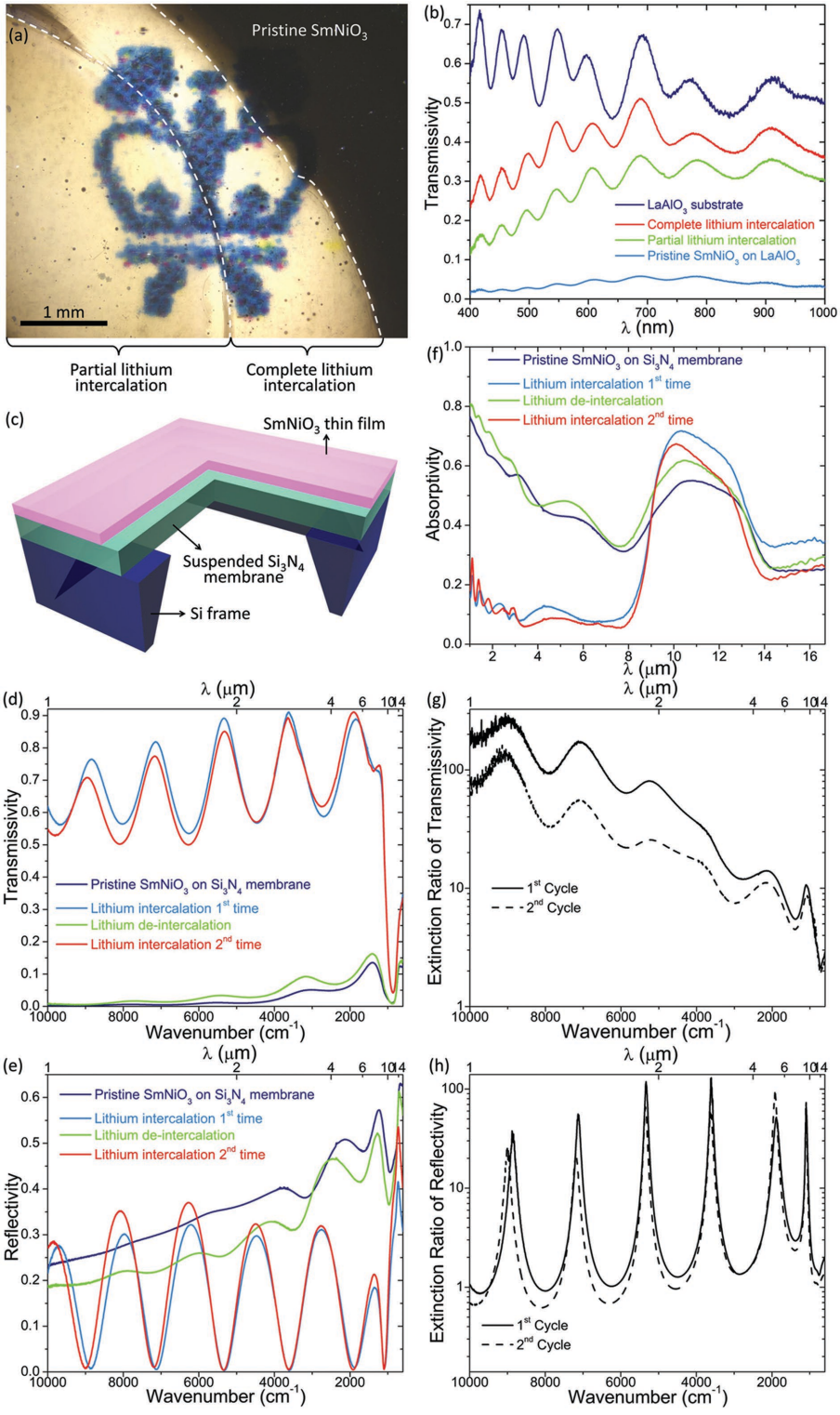

Figure 2. Broadband tuning through the visible, near-infrared, and mid-infrared using thin-film $SmNiO_3$, where the phase transition was realized by lithium intercalation and de-intercalation. a) Optical image of a device placed on top of a Columbia Engineering School logo. The device consists of a 80 nm $SmNiO_3$ thin film deposited on a 500 μm $LaAlO_3$ substrate. Visual transparency can be clearly seen upon electron doping. b) Measured visible and near-infrared transmission spectra taken from different regions of the device. c) Schematic of another device consisting of a 200 nm $SmNiO_3$ film deposited on a 1 μm suspended Si_3N_4 membrane. d–f) Measured transmission, reflection, and absorption spectra of the device in (c), respectively, showing good reversibility and repeatability of the device performance. g,h) Extinction ratio of optical transmission and reflection, respectively, of the device in (c) during two representative cycles of phase transition.

Adv. Mater. **2016**,
DOI: 10.1002/adma.201601204

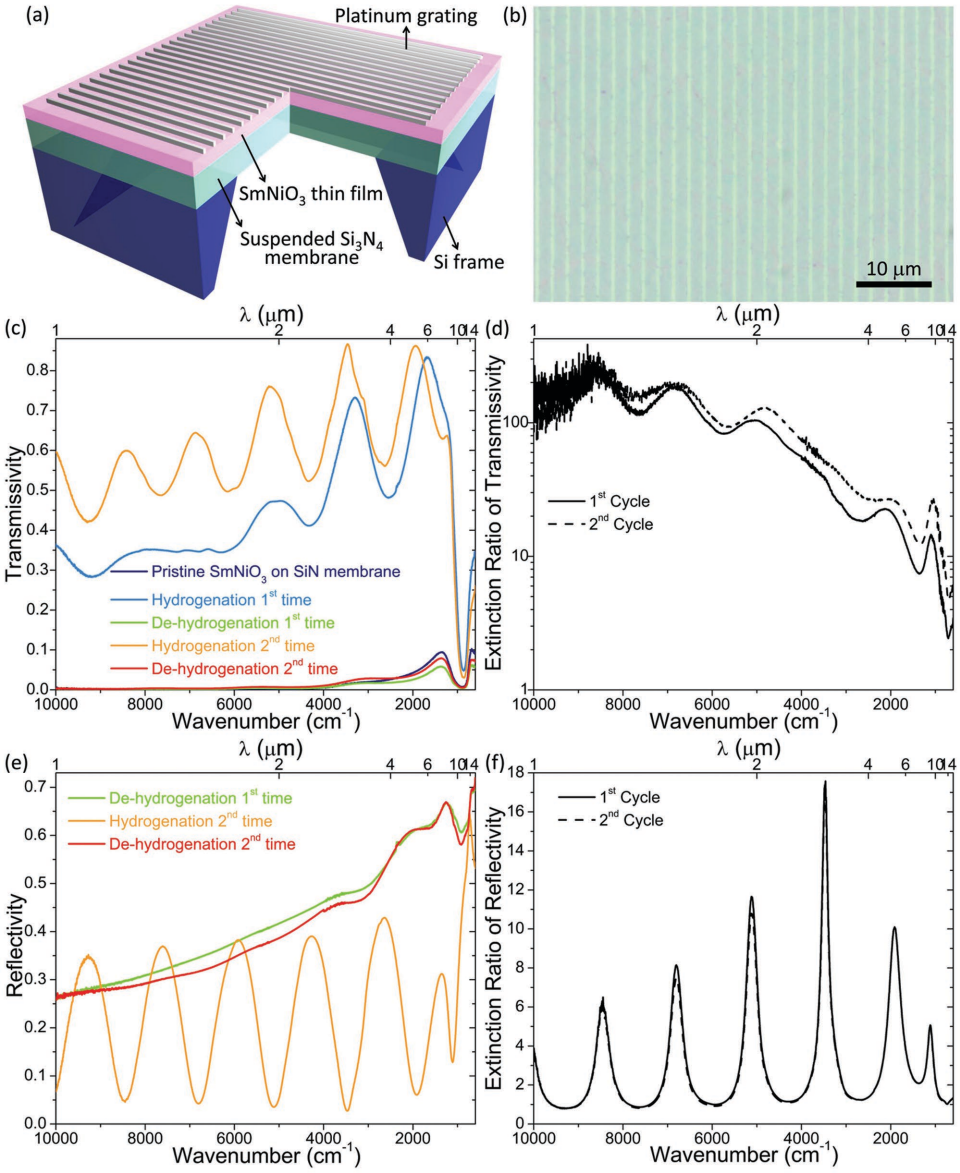

Figure 3. Broadband tuning of near-infrared and mid-infrared transmissivity and reflectivity using thin-film $SmNiO_3$ patterned with a Pt grating, where the phase transition of $SmNiO_3$ was realized by annealing the device in H_2 and O_3. a) Schematic of the device. b) Optical image of fabricated structure. Bright vertical lines are Pt grating fingers with a periodicity of 2 μm. c) Transmission spectra of the device. d) Extinction ratio of optical transmission during two representative cycles of $SmNiO_3$ phase transition. e) Reflection spectra of the device. f) Extinction ratio of optical reflection during two cycles of $SmNiO_3$ phase transition.

Information). When $SmNiO_3$ is at its optically transparent state, incident infrared light generates strong plasmonic resonance in the aperture antennas. The plasmonic resonance manifests itself as strongly localized optical near-fields and oscillating electric currents at optical frequencies in the vicinity of the apertures (Figure 4b). Because of optical losses in the metallic antenna structure and in $SmNiO_3$ (electron-doped $SmNiO_3$ has small but non-zero imaginary part of the complex refractive index), the plasmonic resonance leads to significant absorption of optical power, which results in a dip in the reflection spectra (Figure 4d,f,h). The spectral location of the dip is controlled by the size of the aperture antennas: longer apertures resonantly interact with light with proportionally longer wavelengths. When $SmNiO_3$ is at its pristine state, however, strong optical losses completely damp the plasmonic resonance so that the reflection spectra are featurelessly flat (Figure 4d,f,i). The resonant interaction between light and the aperture antennas leads to substantial tuning within a narrow band of spectrum (Figure 4e,g) while $SmNiO_3$ is switched between the opaque and transparent states. The cross-shaped apertures are chosen because they work for light with arbitrary state of polarization. The Pt back mirror is used to create image dipoles of the aperture antennas. The near-field coupling between the aperture antennas and their image dipoles reduces the radiation losses and leads to narrow spectral features. The narrow spectral feature enables tuning of a narrow band of infrared light or optical

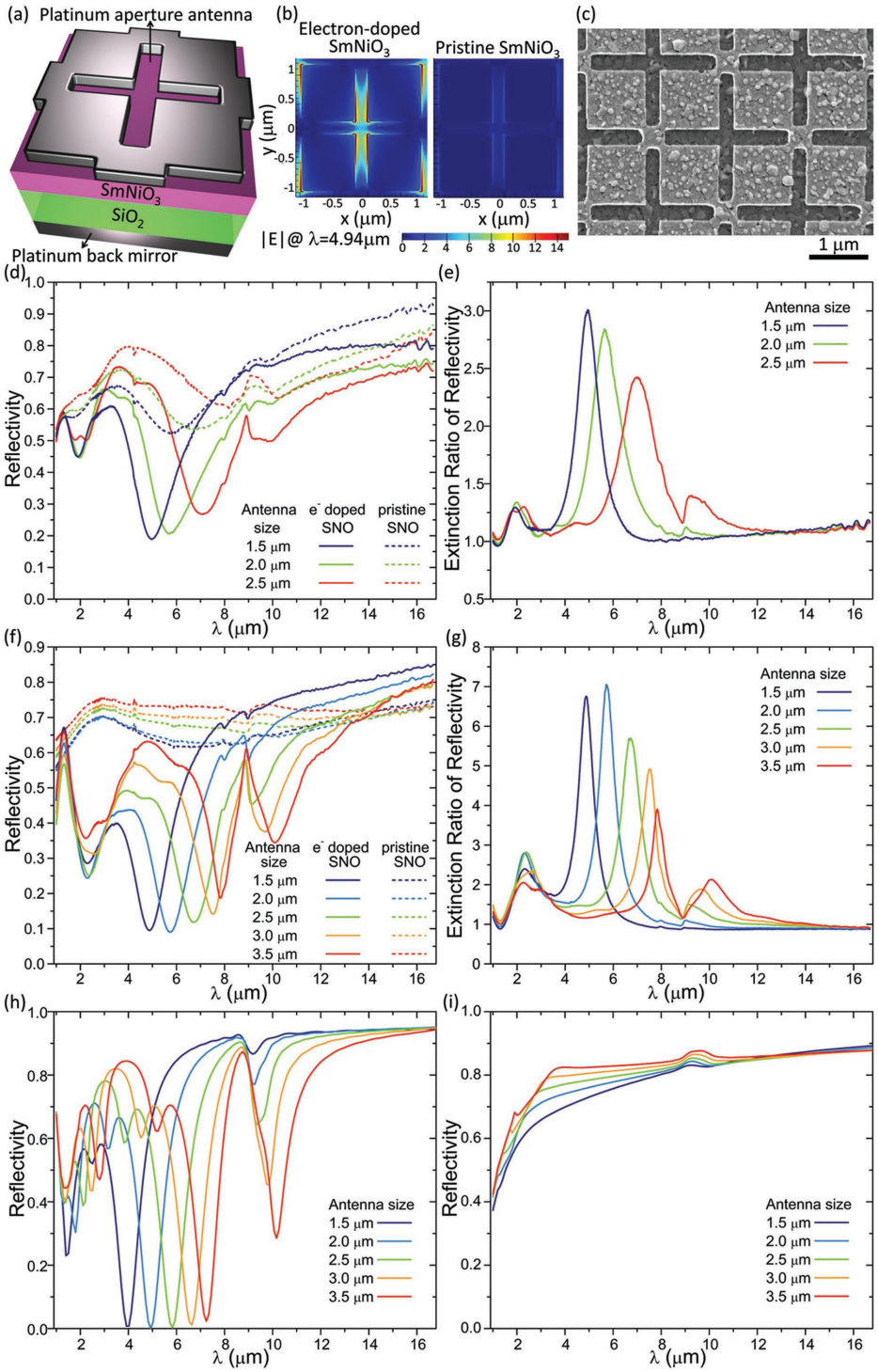

Figure 4. Narrowband tuning of infrared reflectivity in devices consisting of plasmonic metasurfaces patterned on $SmNiO_3$ thin films. a) Schematic of the unit cell of the device consisting of a Pt aperture antenna separated from a Pt mirror by thin films of $SmNiO_3$ and SiO_2. b) Simulations showing optical near-field distributions (i.e., $|E|$) around one aperture antenna. The antenna is 2 μm × 2 μm in size and incident light at $\lambda = 4.94$ μm is polarized along the *x*-direction. Strong plasmonic resonance occurs when $SmNiO_3$ is doped with electrons, while the plasmonic resonance is damped when $SmNiO_3$ is in the pristine state. c) SEM image of part of a device consisting of Pt cross apertures 2 μm × 2 μm in size patterned on $SmNiO_3$. d) Measured reflection spectra of devices where $SmNiO_3$ phase transition was induced by ionic liquid gating. e) Extinction ratio of the reflection spectra in (d), showing large tuning of reflectivity over narrow spectral ranges. The spectral location of peak tuning is determined by the size of aperture antennas. f) Measured reflection spectra of devices where $SmNiO_3$ phase transition was induced by hydrogenation and de-hydrogenation. g) Extinction ratio of the reflection spectra in (f) showing large tuning of reflectivity over narrow spectral ranges. h,i) Simulated reflection spectra when $SmNiO_3$ is at the electron-doped and pristine states, respectively.

Adv. Mater. **2016**,
DOI: 10.1002/adma.201601204

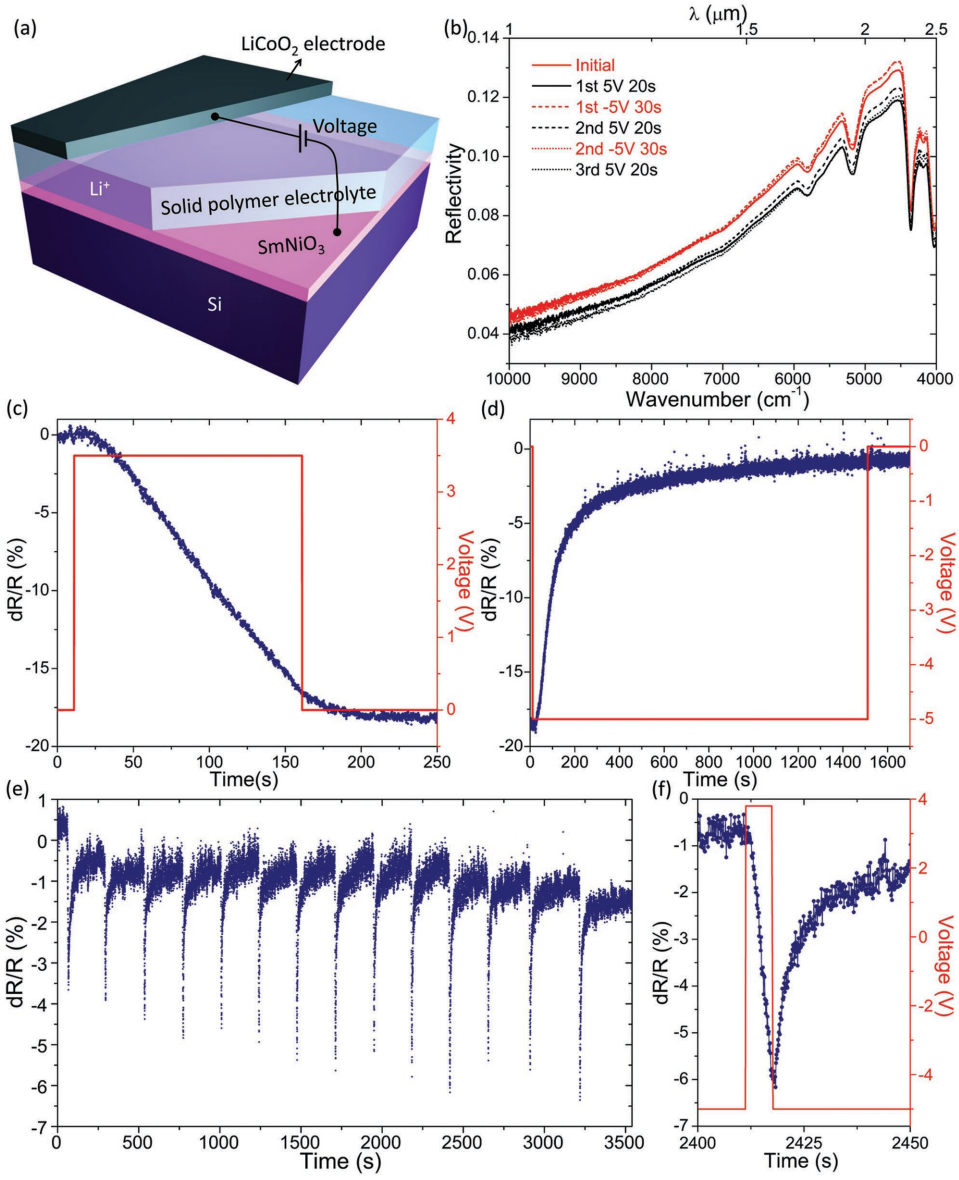

Figure 5. Electrically controllable solid-state electro-optic modulators based on $SmNiO_3$. a) Schematic of the device consisting of a 200 nm $SmNiO_3$ film, a solid polymer electrolyte with high ionic conductivity, and a $LiCoO_2$ electrode. The lithium ions are provided by bis(trifluoromethane)sulfonamide lithium salt (LiTFSI) and the polymer is based on poly(ethylene glycol) (PEG). b) Measured infrared reflection spectra during repeated phase-transition cycles of $SmNiO_3$. c,d) Temporal response of reflectivity at $\lambda = 1.55$ μm during complete lithium intercalation and de-intercalation processes, respectively. e) Temporal response of reflectivity during repeated partial phase-transition cycles of $SmNiO_3$. f) Zoom-in of (e) showing one cycle of modulation.

memory devices that can only be read by light of selected wavelengths. For example, the device patterned with cross apertures 2 μm × 2 μm in size could tune optical reflectivity by a factor of 7 at $\lambda = 5.7$ μm (blue curve in Figure 4g), while the tuning of light at $\lambda > 8$ μm of the same device is insignificant. Figure S3 and S4 (Supporting Information) show repeatability of device performance during several cycles of $SmNiO_3$ phase transition.

To demonstrate the potential of using $SmNiO_3$ in all-solid-state devices, we fabricated devices consisting of 200 nm $SmNiO_3$ films, solid polymer electrolytes (SPEs) containing lithium ions, and $LiCoO_2$ cathodes (**Figure 5**a). The SPE transports lithium ions between the $LiCoO_2$ electrode and $SmNiO_3$ film to induce phase change of the latter. We chose a specific SPE (Section S2.5, Supporting Information) because its high ionic conductivity could accelerate lithium intercalation/de-intercalation cycles and its resistance to lithium dendrite formation could ensure safe operation of the device for many cycles.[27] Our measurements show reversible modulation of reflectivity dR/R = 10%–25% in the wavelength range of $\lambda = 1$–2.5 μm on an area of the solid-state device without the top $LiCoO_2$ electrode (Figure 5b). By applying voltages of +3.5 and −5 V to drive lithium intercalation and de-intercalation processes, respectively, we measured ≈18% modulation of dR/R at the telecommunications wavelength of 1.55 μm (Figure 5c,d).

In this case, bulk phase change of 200 nm $SmNiO_3$ took ≈120 s for the intercalation process and ≈280 s for the de-intercalation process (time constant is defined here as the duration in which relative reflectivity dR/R changes from 0% to 80% of its peak value). If we allow partial phase change of the $SmNiO_3$ film (i.e., phase change only occurs near top layers of the film), the response time can be substantially reduced, while the optical modulation strength decreases correspondingly. For example, a modulated reflectivity $\Delta R/R$ of ≈5.5% at λ = 1.55 μm was achieved when the applied voltage was repeatedly switched between +3.8 and −5 V (Figure 5e,f), and the intercalation time for each cycle was only ≈5 s, while the de-intercalation time was ≈23 s. The response time is limited by the diffusion of lithium ions in the SPE and does not represent the intrinsic response time of $SmNiO_3$ phase transition. The modulation strength can be substantially increased by using optical metasurface structures to enhance light–material interaction. The reflection spectra in Figure 5b were stable after removal of applied voltage, demonstrating the non-volatility of the devices.

Perovskite nickelates as a new platform for photonics has a number of unique and desirable features:

i) The phase change of $SmNiO_3$ is induced by filling-controlled Mott transition[28–30] and there is no crystal symmetry change during the phase-change process.[20–22] This is unlike the structural symmetry breaking seen in the thermal phase transitions of nickelates and VO_2,[31–35] or switching between amorphous and crystalline states in phase-change chalcogenide alloys.[15–19] This quite unusual feature implies that fast switching between the two phases of $SmNiO_3$ is possible, only limited by the speed of carrier injection and removal. We have so far demonstrated a switching time ranging from seconds to minutes in $SmNiO_3$ films a couple hundred nanometers in thickness. The operation speed can be boosted by using nanometer thick $SmNiO_3$ films, and large optical modulation depth can still be achieved by using metasurface structures to enhance the interaction between light and small volumes of $SmNiO_3$. Therefore, $SmNiO_3$ has the potential to be used in planar optical modulators and spatial light modulators that allow for molding optical wavefronts in time and in space.

ii) The phase transition of $SmNiO_3$ is induced by electron doping at room temperature; high-quality $SmNiO_3$ thin films can be reliably synthesized and are stable in ambient conditions. These properties make the material suitable for electric-field tunable solid-state devices and compare favorably to other tunable optical materials where light, temperature, or magnetic field, instead of electric field, is used to change the materials properties. These properties also compare favorably to organic electrochromic materials and some inorganic electrochromic materials (such as $Li_4Ti_5O_{12}$[36]) that are unstable in the presence of oxygen and moisture.

iii) The optically opaque and transparent states of $SmNiO_3$ are highly stable, non-volatile, and its intermediate states with various degrees of transparency can be addressed reversibly by controlling the level of doping. The non-volatile, multi-level optical states of $SmNiO_3$ could be exploited to create reconfigurable, low power planar photonic devices, such as programmable holograms and optical memories.

iv) Strong electron correlation as a result of electron doping in $SmNiO_3$ drastically opens up the optical band gap, and leads to a substantial change in its optical refractive indices over an exceptionally broad spectrum, from the visible to the long-wavelength mid-infrared (Figure 1f). This property has enabled us to experimentally demonstrate tuning of optical reflectivity and transmissivity that is record-breaking in terms of modulation depth and bandwidth (Figure S7 and S8, Supporting Information). The super broadband performance of $SmNiO_3$ and its second-to-minute level phase-change time demonstrated so far could be exploited for applications in smart windows and variable emissivity coatings. Smart windows are traditionally based on electrochromic materials. The change of their optical refractive indices is often not uniformly large over the entire visible and near-infrared spectra, which leads to imperfect control of sunlight. In comparison, we show in simulations that 200 nm $SmNiO_3$ films allow for continuous tuning of optical transmissivity between ≈0.05 and ≈0.6 averaged over λ = 400–2500 nm, where solar energy culminates (Figure S5, Supporting Information). As $SmNiO_3$ shows large tunable absorptivity also in the mid-infrared, it could be an ideal candidate for building variable emissivity coatings, which could find useful applications in infrared camouflage (matching thermal radiation of an object to background thermal radiation) and radiative thermal control of spacecrafts. Figure S6 (Supporting Information) shows the design of a coating that provides variable emissivity between ≈0.09 and ≈0.7 averaged over λ = 4–16 μm.

The electron-doping-induced phase change is expected to be a universal effect for rare earth nickelates as they have similar electronic structure with the extent of band gap modulation dependent on the phase metastability.[37] Therefore, our photonic design can be extended to a wider range of materials. The ease of reversibly inducing the phase change, however, depends on the thermodynamic stability of Ni^{3+} and Ni^{2+} valence state in the material. The stability of Ni^{3+} valence state in the lattice (with respect to Ni^{2+}) is related to the tolerance factor of the perovskite, which is directly associated with the ion size of the rare earth element. With decreasing rare earth ionic radii, it consumes less energy to form Ni^{2+}, but requires more energy to reverse back to the Ni^{3+} state.[37] This provides another degree of freedom that allows us to minimize the switching energy by engineering the Ni valence stability with proper rare earth elements or their alloys.

In summary, we have demonstrated that the phase transition of a model correlated perovskite nickelate $SmNiO_3$ has great potential for active photonic device applications. Large tuning of light using a hybrid structure consisting of plasmonic metasurfaces and thin-film nickelates is demonstrated. Solid-state modulators that are electric-field tunable are also realized. The ability to modulate optical band gap by controlling strong electron correlations in a quantum material without thermal constraints represents a new paradigm for realizing tunable photonic devices.

Adv. Mater. 2016,
DOI: 10.1002/adma.201601204

Experimental Section

$SmNiO_3$ Thin-Film Synthesis: $SmNiO_3$ thin films were grown by physical vapor deposition followed by ultrahigh pressure annealing, which is thermodynamically required for the formation of perovskite phase. Before sputtering, the substrate wafers were cleaned by acetone, isopropyl alcohol, and deionized water and then dried by N_2 gas. The $SmNiO_3$ thin films were deposited by co-sputtering from Sm and Ni metal targets at room temperature. The growth pressure was set at 5 mTorr in a constant flow of 40/10 sccm Ar/O_2 mixture. The d.c. power for the Ni target was adjusted to 75 W and radio frequency power for the Sm target was 150 W to obtain an ≈1:1 Sm:Ni cation ratio, as determined by energy-dispersive X-ray spectroscopy. Growth time ranged from 30 min to a few hours to vary the film thickness. The as-sputtered samples were then transferred to a home-built high pressure vessel. The vessel was then inserted into a tube furnace and annealed at 500 °C for 24 h under 1500 psi pure O_2. Detailed instrumentation information and high pressure thermodynamic conditions for phase formation could be found in ref. [38]. The device fabrication procedure and the method for synthesizing the solid polymer electrolyte can be found in the Supporting Information.

Supporting Information

Supporting Information is available from the Wiley Online Library or from the author.

Acknowledgements

The work was supported by Defense Advanced Research Projects Agency Young Faculty Award (Grant No. D15AP00111), Office of Naval Research Young Investigator Award program (Grant No. N00014-16-1-2442), Air Force Office of Scientific Research (Grant No. FA9550-14-1-0389 through a Multidisciplinary University Research Initiative program, and Grant No. FA9550-12-1-0189), National Science Foundation (Grant No. ECCS-1307948), and Army Research Office (Grant Nos. W911NF-16-1-0042 and W911NF-14-1-0669). Research was carried out in part at the Center for Functional Nanomaterials, Brookhaven National Laboratory, which was supported by the U.S. Department of Energy, Office of Basic Energy Sciences, under Contract No. DE-SC0012704. The authors acknowledge helpful discussions with Yuan Yang.

Received: March 2, 2016
Revised: July 1, 2016
Published online:

[1] H. A. Haus, *Waves and Fields in Optoelectronics*, Prentice-Hall, Englewood Cliffs, NJ, USA **1984**.
[2] R. W. Boyd, *Nonlinear Optics*, 3rd ed., Academic, Burlington, MA, USA **2008**.
[3] V. R. Almeida, C. A. Barrios, R. R. Panepucci, M. Lipson, *Nature* **2004**, *431*, 1081.
[4] Q. Xu, B. Schmidt, S. Pradhan, M. Lipson, *Nature* **2005**, *435*, 325.
[5] J. Park, J.-H. Kang, X. Liu, M. L. Brongersma, *Sci. Rep.* **2015**, *5*, 15754.
[6] V. J. Sorger, N. D. Lanzillotti-Kimura, R.-M. Ma, X. Zhang, *Nanophotonics* **2012**, *1*, 17.
[7] F. Yi, E. Shim, A. Y. Zhu, H. Zhu, J. C. Reed, E. Cubukcu, *Appl. Phys. Lett.* **2013**, *102*, 221102.
[8] Y. Yao, R. Shankar, M. A. Kats, Y. Song, J. Kong, M. Loncar, F. Capasso, *Nano Lett.* **2014**, *14*, 6526.
[9] N. Dabidian, I. Kholmanov, A. B. Khanikaev, K. Tatar, S. Trendafilov, S. H. Mousavi, C. Magnuson, R. S. Ruoff, G. Shvets, *ACS Photonics* **2015**, *2*, 216.
[10] R. J. Mortimer, *Annu. Rev. Mater. Res.* **2011**, *41*, 241.
[11] P. R. Somani, S. Radhakrishnan, *Mater. Chem. Phys.* **2002**, *77*, 117.
[12] K. Sauvet, L. Sauques, A. Rougier, *J. Phys. Chem. Solids* **2010**, *71*, 696.
[13] B.-B. Cui, J.-H. Tang, J. Yao, Y.-W. Zhong, *Angew. Chem., Int. Ed.* **2015**, *54*, 9192.
[14] H.-J. Yen, G.-S. Liou, *Chem. Mater.* **2009**, *21*, 4062.
[15] S. Hudgens, B. Johnson, *MRS Bull.* **2004**, *29*, 829.
[16] M. Wuttig, N. Yamada, *Nat. Mater.* **2007**, *6*, 824.
[17] C. Ríos, M. Stegmaier, P. Hosseini, D. Wang, T. Scherer, C. D. Wright, H. Bhaskaran, W. H. P. Pernice, *Nat. Photonics* **2015**, *9*, 725.
[18] P. Hosseini, C. D. Wright, H. Bhaskaran, *Nature* **2014**, *511*, 206.
[19] Q. Wang, E. T. F. Rogers, B. Gholipour, C.-M. Wang, G. Yuan, J. Teng, N. I. Zheludev, *Nat. Photonics* **2016**, *10*, 60.
[20] J. Shi, Y. Zhou, S. Ramanathan, *Nat. Commun.* **2014**, *5*, 4860.
[21] Y. Zhou, X. Guan, H. Zhou, K. Ramadoss, S. Adam, H. Liu, S. Lee, J. Shi, M. Tsuchiya, D. D. Fong, S. Ramanathan, *Nature* **2016**, *534*, 231.
[22] L. Wang, S. Das, L. Chang, L. You, Y. Feng, X. He, K.-J. Jin, Y. Zhou, H. G. Ong, P. Ren, S. Wang, L. Chen, J. Wang, *ACS Appl. Mater. Interfaces* **2016**, *8*, 9769.
[23] J. R. Howell, R. Siegel, M. P. Mengüç, *Thermal Radiation Heat Transfer*, 5th ed., CRC Press, Boca Raton, FL, USA **2010**.
[24] N. Yu, P. Genevet, M. A. Kats, F. Aieta, J.-P. Tetienne, F. Capasso, Z. Gaburro, *Science* **2011**, *334*, 333.
[25] N. Yu, F. Capasso, *Nat. Mater.* **2014**, *13*, 139.
[26] A. V. Kildishev, A. Boltasseva, V. M. Shalaev, *Science* **2013**, *339*, 1232009.
[27] Q. Pan, D. M. Smith, H. Qi, S. Wang, C. Y. Li, *Adv. Mater.* **2015**, *27*, 5995.
[28] J. H. de Boer, E. J. W. Verwey, *Proc. Phys. Soc.* **1937**, *49*, 59.
[29] N. F. Mott, *Can. J. Phys.* **1956**, *34*, 1356.
[30] N. F. Mott, *Rev. Mod. Phys.* **1968**, *40*, 677.
[31] M. Zaghrioui, A. Bulou, P. Lacorre, P. Laffez, *Phys. Rev. B* **2001**, *64*, 081102.
[32] Z. Yang, C. Ko, S. Ramanathan, *Annu. Rev. Mater. Res.* **2011**, *41*, 337.
[33] M. A. Kats, R. Blanchard, P. Genevet, F. Capasso, *Nat. Mater.* **2013**, *12*, 20.
[34] M. A. Kats, R. Blanchard, P. Genevet, Z. Yang, M. M. Qazilbash, D. N. Basov, S. Ramanathan, F. Capasso, *Opt. Lett.* **2013**, *38*, 368.
[35] M. M. Qazilbash, M. Brehm, B.-G. Chae, P.-C. Ho, G. O. Andreev, B.-J. Kim, S. J. Yun, A. V. Balatsky, M. B. Maple, F. Keilmann, H.-T. Kim, D. N. Basov, *Science* **2007**, *318*, 1750.
[36] M.-S. Song, A. Benayad, Y.-M. Choi, K.-S. Park, *Chem. Commun.* **2012**, *48*, 516.
[37] J. Chen, Y. Zhou, S. Middey, J. Jiang, N. Chen, L. Chen, X. Shi, M. Döbeli, J. Shi, J. Chakhalian, S. Ramanathan, *Appl. Phys. Lett.* **2015**, *107*, 031905.
[38] R. Jaramillo, F. Schoofs, S. D. Ha, S. Ramanathan, *J. Mater. Chem. C* **2013**, *1*, 2455.